Annals of Nuclear Energy 194 (2023) 110066

Contents lists available at ScienceDirect

Annals of Nuclear Energy

journal homepage: www.elsevier.com/locate/anucene

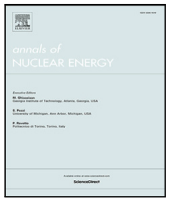

Modeling noise experiments performed at AKR-2 and CROCUS zero-power reactors

M. Hursin [a,e,*], A. Zoia [b], A. Rouchon [b], A. Brighenti [b], I. Zmijarevic [b], S. Santandrea [b], P. Vinai [c], A. Mylonakis [c], H. Yi [c], C. Demazière [c], V. Lamirand [a,e], K. Ambrozic [a], T. Yamamoto [d], S. Hübner [f], A. Knospe [f], C. Lange [f], S. Yum [g], R. Macian [g], A. Vidal [h], D. Ginestar [h], G. Verdú [h]

[a] Ecole Polytechnique Fédérale de Lausanne (EPFL), Lausanne, Switzerland
[b] Université Paris-Saclay, CEA, Service d'Etudes des Réacteurs et de Mathématiques Appliquées, 91191, Gif-sur-Yvette, France
[c] Chalmers University of Technology, Gothenburg, Sweden
[d] Kyoto University, Osaka, Japan
[e] Paul Scherrer Institute, Villigen, Switzerland
[f] Technische Universität Dresden, Germany
[g] Technische Universität München, Germany
[h] Universitat Politècnica de València, València, Spain

ARTICLE INFO

Keywords:
Noise simulators
Validation
CORTEX
Experimental data

ABSTRACT

CORTEX is a EU H2020 project (2017-2021) devoted to the analysis of 'reactor neutron noise' in nuclear reactors, i.e. the small fluctuations occurring around the stationary state due to external or internal disturbances in the core. One important aspect of CORTEX is the development of neutron noise simulation codes capable of modeling the spatial variations of the noise distribution in a reactor. In this paper we illustrate the validation activities concerning the comparison of the simulation results obtained by several noise simulation codes with respect to experimental data produced at the zero-power reactors AKR-2 (operated at TUD, Germany) and CROCUS (operated at EPFL, Switzerland). Both research reactors are modeled in the time and frequency domains, using transport or diffusion theory. Overall, the noise simulators managed to capture the main features of the neutron noise behavior observed in the experimental campaigns carried out in CROCUS and AKR-2, even though computational biases exist close to the region where the noise-inducing mechanical vibration was located (the so-called "noise source"). In some of the experiments, it was possible to observe the spatial variation of the relative neutron noise, even relatively far from the noise source. This was achieved through reduced uncertainties using long measurements, the installation of numerous, robust and efficient detectors at a variety of positions in the near vicinity or inside the core, as well as new post-processing methods.

For the numerical simulation tools, modeling the spatial variations of the neutron noise behavior in zero-power research reactors is an extremely challenging problem, because of the small magnitude of the noise field; and because deviations from a point-kinetics behavior are most visible in portions of the core that are especially difficult to be precisely represented by simulation codes, such as experimental channels. Nonetheless the limitations of the simulation tools reported in the paper were not an issue for the CORTEX project, as most of the computational biases are found close to the noise source.

1. Introduction

The goal of the EU H2020 CORTEX project (2017–2021) (Demazière et al., 2018) is the development of a core monitoring technique capable of identifying and characterizing the source of the 'reactor neutron noise' in an operating nuclear reactor, i.e. the small fluctuations occurring around the stationary state due to external or internal disturbances in the core, based on the available neutron detector time series. Reactor neutron noise is often related to anomalies, whose monitoring is of utmost importance for reactor diagnostics (Pázsit and Demazière, 2010). Information on neutron noise is usually very sparse, as the number of available out-of-core neutron counters, in-core power/flux monitors, thermocouples, and pressure transducers is typically small.

* Corresponding author at: Ecole Polytechnique Fédérale de Lausanne (EPFL), Lausanne, Switzerland.
E-mail address: mathieu.hursin@epfl.ch (M. Hursin).

https://doi.org/10.1016/j.anucene.2023.110066
Received 23 March 2023; Received in revised form 8 July 2023; Accepted 27 July 2023
Available online 18 August 2023

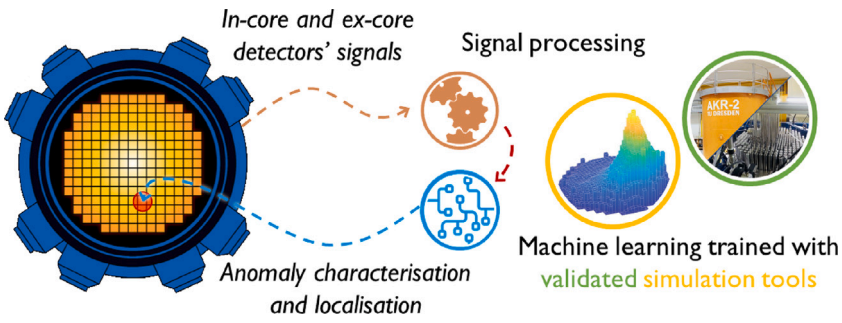

Fig. 1. CORTEX in a picture.

The methodology developed within CORTEX relies on a number of steps, as illustrated in Fig. 1. One of the most important steps is the accurate determination of the reactor transfer function, e.g. the response of the reactor to a given perturbation. With this information in place, it is possible to use an inversion algorithm based on signal processing and machine learning techniques (Stulík et al., 2019; Stefanos et al., 2020; Alexandridis, 2020) to determine the location and type of perturbation causing the signal patterns detected in the time series recorded in the detectors.

The capability to predict the spatial variations of the neutron noise distribution is essential, as the detectors may be located far away from the perturbation or even outside the core.

For the modeling of the reactor transfer function, various solvers have been developed during the CORTEX project, based on different approaches, such as lower- and higher-order deterministic methods and stochastic methods, working either in the time or frequency domain (Vidal-Ferràndiz et al., 2020b, 2022; Vinai et al., 2021b; Zoia et al., 2021; Mylonakis et al., 2021; Rouchon et al., 2019; Yamamoto, 2018). These solvers need to be verified and validated to demonstrate they can provide reliable information when training the machine learning algorithms. Extensive work concerning the verification of the solvers through code-to-code comparisons and the evaluation of low-order methods via reference solutions generated with high-order methods has been done (Vinai et al., 2021a, 2023). The present paper focuses on the validation phase using experimental campaigns conceived specifically for the project (Lamirand et al., 2020c, 2018, 2020b, 2021) at the AKR-2 reactor of the Technische Universität Dresden (TUD) and at the CROCUS reactor of École Polytechnique Fédérale de Lausanne (EPFL).

The paper is structured as follows. In Section 2, the strategy of the validation work is discussed. In Section 3, the generation of experimental data at AKR-2 and CROCUS is briefly presented. In Section 4, a brief description of the solvers as well as the associated research reactor models is provided, and in Section 5 the experimental and calculated neutron noise are compared. In Section 6, conclusions are provided.

2. Validating noise simulators within CORTEX

In order to produce a training dataset for the machine learning algorithms within CORTEX, the use of a large amount of earmarked information is needed, i.e. clean detector time series for which the perturbation is precisely known. Generally speaking, the use of power reactor data is not practical, as it is usually not earmarked (the shape and location of the "noise source", e.g., possible mechanical vibrations, are not known), it is sparse (not enough detectors) and it is also scarce (not enough reactor cycles available). To achieve the goal envisioned in the project (training machine learning algorithms with high degree of spatial accuracy), the number of detectors typically available in power reactors is too low. This also the case for zero-power research reactors.

As a result, it was decided early in the project to use models (neutron noise simulators) to produce synthetic data. In order to make sure that the codes produce reliable data, a comparison to experimental measurements is carried out using dedicated experimental campaigns (known noise source, large number of detectors and measurements) conceived and carried out for the purposes of the project.

A meaningful comparison between simulations and measurements requires various ingredients. First, quantities of interest (QoI) need to be defined, which are pertinent to the envisioned application of the models. For the CORTEX project, the target application is the training of the machine learning algorithms. Second, estimates of these QoI need to be produced from the codes output and post-processed from the measured quantities. Third, both modeled and measured QoI need to be complemented by uncertainty estimates so that the deviations between the QoI can be put in perspective. The present section focuses on the definition of the QoI.

2.1. Quantities of interest

For core monitoring purpose, the spatial distribution of the amplitude of fluctuations in the neutron detector signals is extremely useful. Those fluctuations are called "neutron noise". The amplitude of the neutron noise at a detector location is the relevant quantity of interest and should be the desired QoI for the validation exercise in CORTEX. It should be noted that the phase of the neutron noise could also provide very relevant information especially for power reactors, see for example Adorjan et al. (2000).

Even if the absolute and relative (to the mean of the signal) amplitude of the fluctuations are of interest, the relative fluctuations are chosen in this work as they are easier to measure since the knowledge of the detector efficiency is not required. Moreover, from a representation point of view, relative fluctuations allow magnifying the deviations of the spatial distribution of the noise from the fundamental mode, as shown in Section 2.1.3.

In CORTEX, the experimental data of neutron noise to be used in the validation of the simulators is produced using zero-power research reactors, where neutron population fluctuations are induced through two main types of neutron noise sources (Lamirand et al., 2020a). The first type (used in AKR-2) is an absorber of variable strength, obtained from the rotation of a piece of Cadmium whose absorption reaction rate varies with respect to the rotation angle (Hübner et al., 2020). The second type (used on both AKR-2 and CROCUS) is a mechanical vibration. In AKR-2, the mechanical vibration consists in a neutron absorber that moves linearly back and forth in an experimental channel located in the vicinity of the reactor core. In CROCUS, the mechanical vibration is induced by moving fuel rods (COLIBRI program) (Lamirand et al., 2020a).

On the modeling side, there are two main approaches to determine the noise amplitude at a given location, based on a given noise source. In the first approach, the codes make use of the formulation of the linearized neutron noise equation in the frequency domain and thus determine the neutron noise as a complex quantity, for each discrete harmonic of the noise source spectrum (the forcing function as seen by the reactor core). The noise sources specific to a given perturbation pattern in the core (each with different frequency spectra) are

combined using the linearity assumption. In the second approach, the code calculates the evolution of the spatial distribution of the flux as a function of time by solving the time-dependent neutron transport equation (or its diffusion approximation) coupled to the evolution of the delayed neutron precursors, for a given perturbation pattern. Both approaches have been developed in the neutron noise solvers conceived during the CORTEX project.

The appropriateness of the diffusion approximation when solving the transport equation have been investigated in the CORTEX project (see for example Vinai et al., 2023). The main conclusions of these investigations is that diffusion is a reasonable approximation far from the noise source, similarly to the case of regular static reactor physics calculations.

The phrasing 'linearity assumption' refers here to the standard 'orthodox linearization' that is assumed by all numerical solvers for the noise equations working in the frequency domain, in order to make the equations more tractable. This assumptions consist in dropping from the Fourier-transformed noise equations all the terms containing products of perturbed quantities. The validity and limitations of this approach have been recently discussed in Zoia et al. (2021). On the contrary, numerical solvers working in the time domain do not need this assumption (Vidal-Ferràndiz et al., 2020a). Harmonics emerge for both the noise equations in the frequency domain, and for the Fourier transform of the noise equations in the time domain: because of the 'orthodox linearization', though, differences in the spectral content of two approaches might differ. Previous analyses have shown that such differences typically concern higher harmonics, whereas the first noise harmonic is very similar for both kinds of numerical solvers (Zoia et al., 2021).

On the experimental side, the noise detectors used to monitor the neutron fluctuations during the measurement campaigns produce time series that must be then post-processed in order to generate information in the frequency domain. For the purpose of this work, time and frequency domain results are compared in terms of neutron noise amplitude and phase at the detector locations. The consistency of time and frequency domain analysis is investigated in Section 2.1.1.

The frequency content of the noise sources involved in this work is not monochromatic, as shown in Lamirand et al. (2020a), since several components appear at frequencies multiple of the excitation frequency ω_0. Nonetheless, in this work we have decided to investigate the first noise harmonic corresponding to ω_0, which in the experimental configurations examined here represents the dominant contribution to the noise spectrum in the frequency domain. Higher harmonics of this excitation frequency were considered in the project (Zoia et al., 2021; Ambrozic, 2021).

Another subtlety with the determination of the QoI concerns the type of quantity provided by the codes and the measurements. The measurement data naturally include the effects of the detector themselves; on the simulation side, on the other hand, some of the noise solvers are capable of taking into account the presence of the detectors on neutron transport, whereas other solvers can only compute the flux fluctuations in coarse regions of the geometry without explicitly modeling the detector. This is certainly a source of bias for the validation exercise. Its magnitude is investigated in Section 5.

2.1.1. Determination of the relative noise characteristics

For the noise solvers working in the frequency domain, the output of the codes is the noise field $\delta\phi_i(\omega)$ over a detector region of index i (a cell of a spatial mesh, or a volume for a Monte Carlo code), possibly decomposed into several energy groups. In most cases met in applications, $\delta\phi_i(\omega)$ is actually a sum over discrete Fourier harmonics, each corresponding to a frequency that is a multiple of the forcing frequency ω_0: this is typically the case of mechanical vibrations (Zoia et al., 2021; Ambrozic, 2021). The relative noise is obtained as follows:

$$\delta\phi_{rel,i}(\omega) = \frac{\delta\phi_i(\omega)}{\phi_0(r_i)} \tag{1}$$

where $\phi_0(r_i)$ is the static value of the response considered (flux, reaction rate), at the location of interest r_i. $\delta\phi_i$ represents the signal fluctuations around its mean. The QoI is thus obtained directly.

For codes working in the time domain, as well as for experiments, the determination of the relative noise from time series is sketched below to provide a general idea of the approach. We refer the reader to Ambrožič et al. (2023) for a thorough description of the processing of experimental time series; for the noise simulators in the time domain, see Vidal-Ferràndiz et al. (2020a), Brighenti et al. (2022).

The detector response to the neutron noise source is proportional to the reactor power at that time. It is therefore desirable to eliminate the power drift by subtracting the mean from the temporal fluctuations. Then, to obtain a relative quantity, the resulting time series is divided by its mean. The processed time series for a detector i is finally given by:

$$S_{N,i}(t) = \frac{S_i(t) - \bar{S}_i}{\bar{S}_i}, \tag{2}$$

where $S_i(t)$ is the original detector signal, $S_{N,i}(t)$ the normalized signal, and $\bar{S}_i$ the mean detector signal. In this work $\bar{S}_i$ was determined as the moving average over a number of oscillation cycles, 10 by default, but could be provided by the user of the code used for the analysis. The effect that this procedure has on the frequency response of the signal is provided in details in Ambrožič et al. (2023). Since our quantities of interests are ratios (see Section 2.1.2) taken in the same frequency range, the response of numerator and denominator is affected by the same factor, which in turn minimizes the possible effects on the ratio.

Next, a Fourier analysis of the normalized signal is carried out to characterize the amplitude and phase of the noise:

$$\delta\phi_{rel,i}(\omega) = FFT[S_{N,i}(t)], \tag{3}$$

where FFT stands for Fast Fourier Transform (Heideman et al., 1984). In general, the FFT-transformed signal in the frequency domain will contain a superposition of harmonics, each corresponding to multiples of the forcing frequency ω_0. The precise shape of the harmonics and their relative amplitude depend on several factors, encompassing the kind of noise source (mechanical vibrations, oscillations, etc.), and the possible symmetries of the detectors (Zoia et al., 2021; Ambrozic, 2021). In the analysis carried out in this work, we will focus exclusively on the noise harmonic at $\omega = \omega_0$: investigations have shown that it is legitimate to neglect higher harmonics.

It is not obvious that the right hand side of Eqs. (1) and (3) represent the same quantity. Starting from the raw signal $S_i(t)$ of detector i, one can express it as a function of the neutron flux at the detector location through the detection efficiency ϵ_i:

$$S_{N,i}(t) = \epsilon_i \phi(r_i, t). \tag{4}$$

It is assumed that the detector efficiency does not depend on time nor space, which is a reasonable assumption far from the noise source (the spectrum does not change over time at the detector location).

The mean detector signal can be defined as:

$$\bar{S}_i = \epsilon_i \phi_0(r_i). \tag{5}$$

By subtracting its mean from the detector signal, one can express the signal fluctuations with respect to its zero-mean (using standard notations of Pázsit and Demazière, 2010):

$$S_{N,i}(t) - \bar{S}_i = \epsilon_i \left(\phi(r_i, t) - \phi_0(r_i)\right) = \epsilon_i \delta\phi(r_i, t). \tag{6}$$

By further dividing by the mean detector signal, one obtains:

$$\frac{S_{N,i}(t) - \bar{S}_i}{\bar{S}_i} = \frac{\epsilon_i \delta\phi(r_i, t)}{\epsilon_i \phi_0(r_i)} = \frac{\delta\phi(r_i, t)}{\phi_0(r_i)}. \tag{7}$$

Taking the FFT of Eq. (7) leads to a quantity that is comparable to the relative noise as computed by the noise simulators in the frequency domain (see Eq. (1)). The results of the FFT stemming from the time-signal might still differ from the Fourier-domain formulation of the

noise equations, because of discretization errors in the time series from experimental measurements: if the series is not "fine" enough, or "long" enough, spurious effects might appear, inducing discrepancies between the two approaches.

2.1.2. Determination of convenient metrics

The quantity $\delta\phi_{rel,i}$ in Eqs. (1) and (3) is not directly useful as QoI for the validation exercise, since it is a complex quantity whose physical interpretation is not obvious. However, the associated power spectral density (see Eq. (8)) is a measure of the noise power at a given frequency. Therefore, the analysis presented in this work will rely on a comparison of the power spectral densities

$$PSD_{i,i}(\omega) = (\delta\phi_{rel,i}(\omega))(\delta\phi_{rel,i}(\omega))^{\dagger}, \tag{8}$$

where $\delta\phi_{rel,i}$ is the relative noise, i identifies a detector location, and the symbol † is for the complex conjugate value. This quantity defines the Auto Power Spectral Density (APSD). Instead of considering only a single detector, it is possible to correlate the noise characteristics of two detectors i and j to obtain the Cross Power Spectral Density (CPSD):

$$CPSD_{i,j}(\omega) = (\delta\phi_{rel,i}(\omega))(\delta\phi_{rel,j}(\omega))^{\dagger}. \tag{9}$$

CPSD is a better metric than APSD as it allows filtering some of the electronic noise of each detector, which is a source of bias in experiments. It should be noted, however, that both APSD and CPSD might suffer from boxcar window effects, which will result in deviations between simulations and measurements. These biases are not considered in this work.

Finally, the CPSD amplitudes generated by the post-processing tools cannot be compared directly, since a normalization constant is involved: for this reason, we have chosen to take the ratios of CPSDs amplitudes as the QoI for the validation exercise. Such ratio is expressed as:

$$QoI_j(\omega) = \frac{\left|CPSD_{i,j}(\omega)\right|}{\left|CPSD_{i,ref}(\omega)\right|} = \sqrt{\frac{\left|APSD_j(\omega)\right|}{\left|APSD_{ref}(\omega)\right|}}. \tag{10}$$

The indices i and j represent two distinct detector locations. The reference detector (denoted by the subscript '*ref*') is a third detector location, chosen as far as possible from the noise source, to reduce both the magnitude of spatial variation of the relative neutron noise (see Section 2.1.3 for details) and possible spectral effects mentioned for detectors located near the noise source. The quantity on the right hand side of the second equal sign of Eq. (10) is used nn the computational side.

From an experimental point of view, the right hand side of the second equality sign in Eq. (11) is used. Instead of choosing i in an arbitrary manner, a weighted sum is computed, where the weight of a given detector i is based on its CPSD ratio uncertainty. Each detector location i can be used to compute $QoI_j(\omega)$. It is desirable to determine a CPSD ratio based on a mean of multiple estimates as it allows reducing significantly the uncertainties. With respect to the CPSD ratio uncertainty, it relies on a bootstrapping approach with the standardized time series. The sections of the signal used for boostrapping are truncated based on the recorded movement of the noise source (usually a finite number of cycles). The full CPSD ratio probability distribution is obtained from the bootstrapping process which allows determining its maximum likelihood as well as the confidence intervals instead of relying on a Gaussian approximation (see Ambrožič et al., 2023 for the full details).

$$QoI_j(\omega) = \sqrt{\frac{\left|APSD_j(\omega)\right|}{\left|APSD_{ref}(\omega)\right|}} \approx \sum_i a_i \frac{\left|CPSD_{i,j}(\omega)\right|}{\left|CPSD_{i,ref}(\omega)\right|}, \tag{11}$$

where a_i is the weight associated with the detector i. It is inversely proportional to the experimental uncertainty. The quantity after the first equal sign represents the QoI from a computational perspective, while the quantity after the second equal sign represents the QoI from an experimental point of view.

Besides the amplitude at a given frequency, the phase between the detectors i and *ref* was also considered, as it is a relevant metric for core monitoring purposes (Adorjan et al., 2000). Given that only one type of noise source is involved in each experiment and given the small size of the research reactors involved, no large phase differences are expected in the observed neutron noise signals; therefore the paper will focus mainly on the amplitude as QoI, while succinctly discussing the phase results.

Nonetheless, for the sake of completeness, a short presentation of how the phase is computed is provided in the following. For the experimental determination of the phase, see e.g. Lamirand et al. (2023b,a). The phase φ is defined as

$$\varphi_j(\omega) = arg(\delta\phi_{rel,j}(\omega)) - arg(\delta\phi_{rel,ref}(\omega)). \tag{12}$$

2.1.3. Spatial variations of the noise characteristics

Using the standard notations of Pázsit (1977), the absolute noise at a given position r and at a time t is given by :

$$\delta\phi(r,t) = \phi_0(r)\delta P(t) + \delta\psi(r,t). \tag{13}$$

The first term on the right hand side represents the point reactor term driven by the reactivity worth of the perturbation. Its spatial dependence is determined by the spatial variation of the fundamental flux distribution ϕ_0. The spatial dependence of the second term is determined by the non-uniform character of the perturbation. In the CORTEX project, the latter term will be used in power reactors for inferring the position of the perturbation.

Expressed in relative terms, the previous equation becomes:

$$\frac{\delta\phi(r,t)}{\phi_0(r)} = \delta P(t) + \frac{\delta\psi(r,t)}{\phi_0(r)}. \tag{14}$$

An important aspect for the visualization of the results (and the definition of the QoI) is apparent from Eq. (14): while the point-kinetics component of the absolute noise follows the fundamental mode ϕ_0, it does not depend on r when considering the relative noise distribution. As a result, any spatial variation shown in the relative noise distribution can be attributed to the ratio between the space dependent component of the noise and the static flux, and thus to the existence of a space-dependent component in the relative noise.

The difference between absolute and relative noise distributions for the thermal flux is illustrated in Fig. 2 for the case of AKR-2 reactor. More information about the AKR-2 and the specific experiment illustrated in Fig. 2 will be provided in Section 3. The noise distribution shown in Fig. 2 corresponds to mechanical vibrations in the periphery of the core (depicted by the black circle).

While the spatial distribution of the absolute neutron noise is similar to the fundamental mode (it has a peak in the core center; the experimental channels are also visible), the relative distribution has a peak at the location of the noise source, and a spatial dependence is observed. As one might expect, away from the noise source the magnitude of the variations is small.

The distribution of the QoI for the thermal flux computed with CORE SIM+ is shown in Fig. 3. The location of the detectors is shown in white, the reference detector in red. Variations of the QoI in the 10% range are expected at detector locations.

Reverting to the expression of the QoI in Eq. (11), one can notice that the ratio will be 1.0 at any point of the reactor if the reactor behaves in a point-like manner, e.g. the space-dependent component of the relative noise is negligible.

As a consequence, deviations of the QoI from 1.0 are observed only if a spatial component of the noise exists (in the sense of Eq. (13)). However, we have no information about the magnitude of the spatial component. Transferring the expression for the relative noise at any detector location in the frequency domain, computing the APSD (the

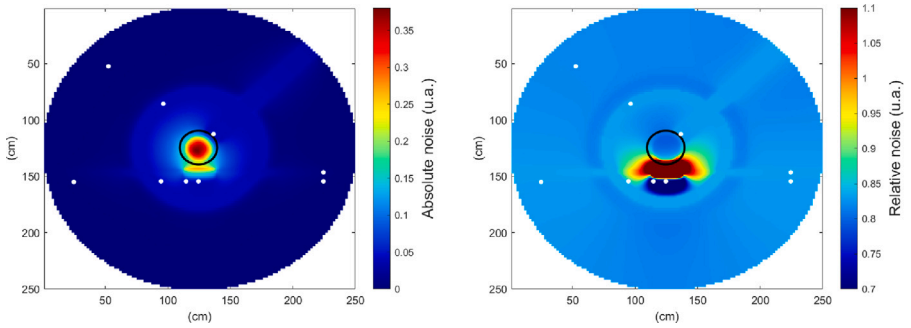

Fig. 2. Absolute (left) vs. Relative (right) thermal noise distribution in AKR-2 8 cm below the core center; triggered by mechanical vibrations, modeled with one of the solver involved in this work (CORE SIM+, see Section 4 for details). The black circle represents the core boundaries.

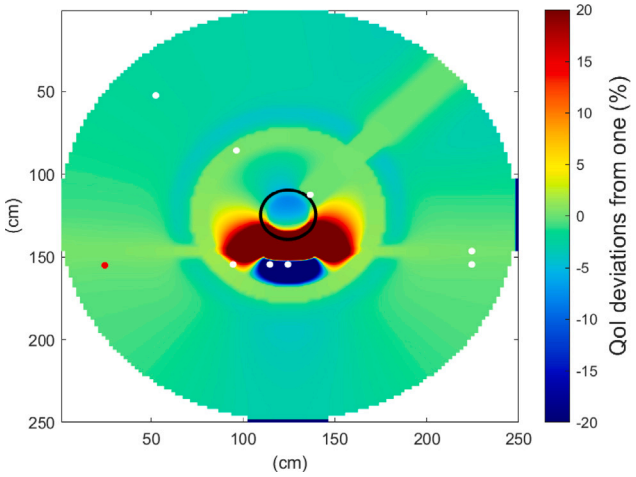

Fig. 3. Spatial variation of the QoI in AKR-2 triggered by mechanical vibrations, modeled with CORE SIM+. The black circle represents the core boundaries. The red dot represents the location of the reference detector.

arguments are dropped for conciseness), and finally using the relationship between point kinetics and spatial components of the noise leads to

$$APSD = |\delta P|^2 + \frac{|\delta\psi|^2}{\phi_0^2} + \frac{1}{\phi_0}(\delta P^\dagger \delta\psi + \delta P \delta\psi^\dagger), \tag{15}$$

where ϕ_0 is the fundamental mode response, δP is the point kinetic component of the noise and $\delta\psi$ is the spatial component of the noise. Assuming that the reference detector is properly chosen, the spatial component of the noise will be negligible and the QoI becomes:

$$QoI = \sqrt{1 + \frac{|\delta\psi|^2}{|\delta P|^2\phi_0^2} + \frac{2}{\phi_0}\Re\left(\frac{\delta\psi}{\delta P}\right)}. \tag{16}$$

where $\Re$ is the real part of a complex quantity. From this expression, it appears that the deviation of the QoI from 1.0 is a non-trivial function of the spatial component of the relative noise. The QoI is equal to 1.0 if the spatial component of the relative noise is zero, or if the condition $\frac{|\delta\psi|^2}{|\delta P|^2} = -2\phi_0\Re\left(\frac{\delta\psi}{\delta P}\right)$ is satisfied.

As $\delta\psi$ is a function of space and δP is not, this condition cannot be satisfied everywhere in the problem. As a result, the deviations from 1.0 observed in Fig. 3 demonstrate the existence of a non-zero spatial component. However, the data shown in this figure does not provide direct quantitative information about the magnitude of the spatial component with respect to the point kinetics one as the RHS of Eq. (16) does not show a simple dependence on $\delta\psi$.

One of the main objectives of the validation exercise is to demonstrate that the noise simulators can predict the spatial component of the relative noise. An agreement of the QoI obtained from simulations and measurements will fulfill this goal, even if the magnitude of the spatial component is not precisely determined; given the magnitude of the deviations shown in Fig. 3, the uncertainty associated with the measurements of the QoI needs to be small.

3. Generation of experimental data at the research reactors

In this section, the experiments carried out within the CORTEX project for the purpose of the validation exercise are summarized. More details about the experimental campaigns at the research reactors can be found in the project deliverables (Lamirand et al., 2021, 2018, 2020b) and especially in their overview in Lamirand et al. (2023b,a).

In the CORTEX project, two types of noise sources have been examined in the research reactors:

- Absorber of Variable Strength (AVS), i.e. an absorber at a given location but with a time-dependent reactivity worth (AKR-2).
- Mechanical vibrations (MV), e.g. a component of the core with time-dependent location – achieved here using linearly moving absorbers (AKR-2 and CROCUS), and a fuel rods oscillator (COLIBRI device Lamirand et al., 2020a).

3.1. Experiments at AKR-2

Throughout the three campaigns carried out during the project, the experimental setup in AKR-2 was improved by the use of a high-precision perturbation linear motor axis (Hübner, 2018), as well as by an increase in the number of detection channels (and their reliability). This latter point was achieve through the development of an FPGA-based acquisition system. Moreover the positioning of detectors with respect to the core and perturbations evolved to allow measurements

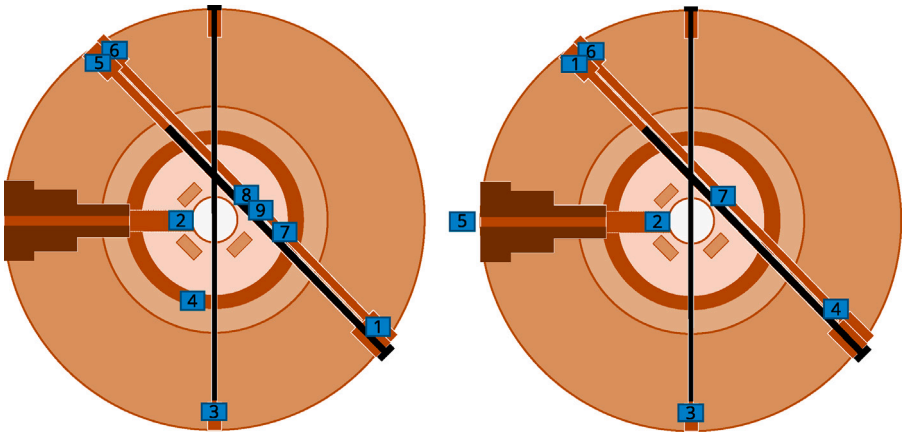

Fig. 4. Detectors setup during the second (left) and third (right) experimental campaigns at AKR-2.

Table 1
Selected experiments done at AKR-2 for comparisons between experiments and simulations.

Type	Excitation frequency (Hz)	Location w.r.t. core center (cm)	Amplitude (cm)	Repetitions	Identifier/Campaign number
AVS	2	23.4	–	6	Exp. #21 (Lamirand et al., 2020b)/2nd
MV	2	5.5	3	4	Exp. #20 (Lamirand et al., 2020b)/2nd

closer to the core thanks to a new detection technology based on miniature scintillators developed by EPFL (see Vincent et al., 2021; Vitullo et al., 2020 for more details). Finally the development of a robust and consistent post-processing methodology allowed for a more reliable estimation of experimental uncertainties in the quantities of interest (Ambrožič et al., 2023).

In the first experimental campaign at AKR-2, the data acquisition systems (DAQs) available at TUD and EPFL were successfully compared with the industry-grade ISTec Sigma system (Rais et al., 2019).

The validation exercise for AKR-2 focused on a subset of the measurements from the second and third campaigns of AKR-2. An overview of the corresponding detector setups is displayed in Fig. 4. Various types of detectors were used, aimed at performing measurements as close as possible to the core. During the third campaign, one miniature fission chamber was placed in the center of channel 3–4 (detector position #8 in Fig. 4).

The first experiment considered used the AVS as perturbation at a rotation frequency of 2 Hz. The second experiment is an off-center MV perturbation with an amplitude of ±3 cm and an oscillation frequency of 2 Hz. Both configurations were repeated 6 times for the AVS and 4 times for the MV during the two experimental campaigns. The relevant parameters for each measurement are summarized in Table 1. In general, detector #1 is chosen as reference detector due to its location far away from the core; and because it is not located in the same channel as the perturbation device.

The choice of the frequency was driven by practical aspects, e.g. to have a reasonable acquisition lengths and low experimental uncertainty. With respect to the MV experiment, an off-center location was chosen to allow for easier convergence of the Monte Carlo simulation (which is notably problematic for this sort of problem (Vinai et al., 2023)). This will however have a detrimental effect, as it will magnify the point-kinetics component of the neutron noise. The large amplitude of the movement is chosen so to improve the signal-to-noise ratio and reduce the experimental uncertainties as much as possible.

In general, small deviations from 1.0 of the QoI are recorded, e.g. less than 20%. One noticeable exception is the detector #3 during MV experiments: as the detector is facing directly the noise source, large deviations (QoI > 5) are observed. With respect to the phase, larger than expected deviations from zero have been reported during the second experimental campaign. These deviations are due to a synchronization issue of the different DAQs involved, the issue was resolved during the third campaign.

The uncertainty estimates associated with AVS and MV measurements were approximately between 5% and 25% during the second campaign; and were further reduced between 3% and 18% during the third one. The magnitude of the experimental uncertainty is tightly related to the detector efficiency and the type of noise source involved. The uncertainty estimates have been confirmed through repetition of the same measurements. This is illustrated in Fig. 5: the spread of the experimental results through their repetition fits within the 'propagated' experimental uncertainties. This gives confidence that the experimental uncertainties are reliable.

3.2. Experiments at CROCUS

In the framework of the CORTEX project, the COLIBRI device (Lamirand et al., 2020a) is used to act as a noise source in the CROCUS zero-power research reactor of EPFL by oscillating fuel rods. COLIBRI is located at the West edge of the reactor and can simultaneously displace up to 18 fuel rods. The amplitude of the oscillation can be selected between the values of ±0.5 mm and ±2.5 mm; and the oscillation frequency up to 2 Hz for selected amplitudes.

An overview of the detectors setup during the three experimental campaigns at CROCUS is displayed in Fig. 6. They are located mostly at the core periphery, with a few of them located in-core (red disk), especially during the second and third campaigns.

The validation exercise for CROCUS is focused on a subset of the measurements listed in Table 2. Detectors #5 and #12 are the reference detectors during the first and second campaign, respectively, as they are at distance and are thus assumed to experience global behavior only. See Lamirand et al. (2018, 2020b, 2021) for the exact numbering of the detectors in each experimental campaign. The choice of the frequency was driven by practical aspects, e.g. to have reasonable acquisition lengths and low experimental uncertainty, while allowing for the effect of water level fluctuations due to the fuel rod movements to be limited and taken into account. Indeed, these fluctuations are negligible at 0.1 Hz, and range about 0.2 mm at 1 Hz (i.e., about 0.8 pcm).

4. Modeling the research reactors

Different neutron noise solvers have been used to simulate the AKR-2 and CROCUS experiments, i.e.

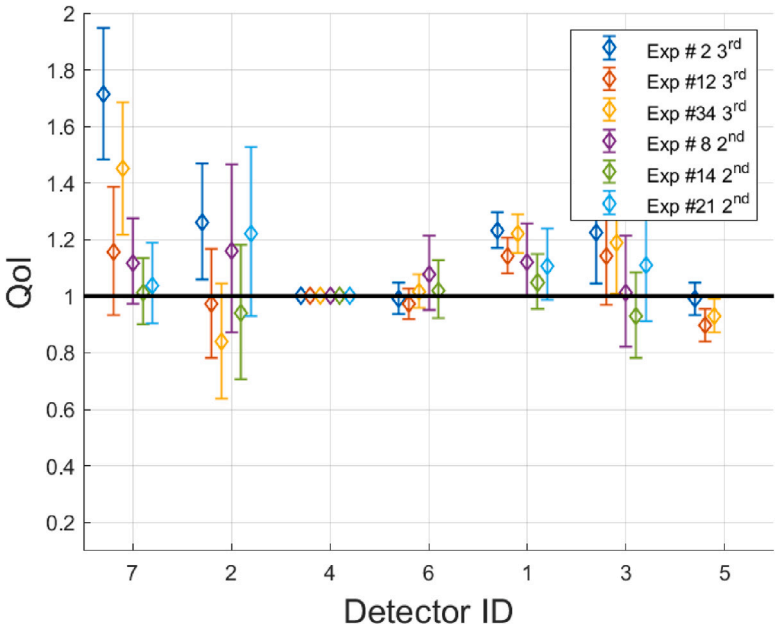

Fig. 5. Repetitions of the same AVS experiment during the second and third campaign at AKR-2. The detectors ID correspond to the third campaign. Det #4 is used as reference detector (it has the same location than Det #1 during the second campaign). The error bars represent a 1σ uncertainty.

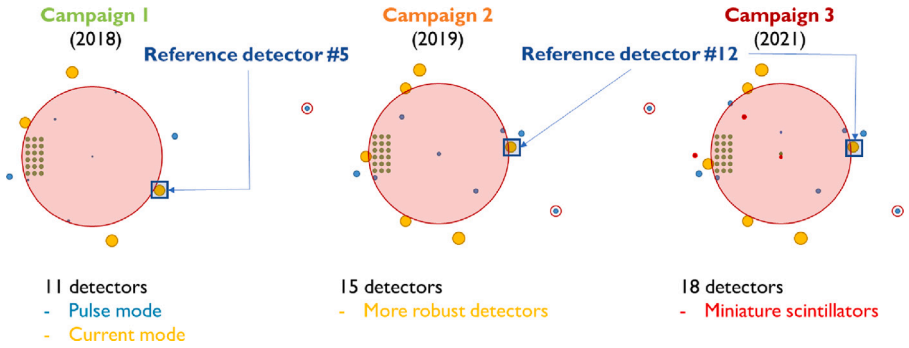

Fig. 6. Detectors setup during the three experimental campaign at CROCUS. The dark green circles represent the oscillating fuel rods.

Table 2
Selected experiments done at CROCUS for comparisons between experiments and simulations.

Power (W)	Excitation frequency (Hz)	Selected amplitude (mm)	Identifier/Campaign number
1	0.1	2	Exp. #12 (Lamirand et al., 2018)/1rst
1	0.1	1.5	Exp. #7 (Lamirand et al., 2020b)/2nd
1	1	1.5	Exp. #8 (Lamirand et al., 2020b)/2nd

- The Monte Carlo code TRIPOLI-4® developed at CEA. The spatial distribution of the noise is determined based on a Monte Carlo solution of the continuous-energy transport equation in the frequency domain (Rouchon et al., 2017, 2019). The noise equations are solved by transporting particles carrying two statistical weights, one for the real part and one for the imaginary part of the noise field. Particle flights are sampled from an exponential distribution, as for the regular Boltzmann equation, whereas the collision events are modified by the presence of complex operators in the noise equations, i.e., an additional imaginary absorption cross section and a complex delayed neutron yield. Such terms are dealt with by correspondingly modifying the probabilities of collision events and the correction factors applied to the statistical weights. For on overview of the algorithms, see Rouchon et al. (2017, 2019).
- The transport-based noise solver of APOLLO3® developed at CEA based on Improved Point-Kinetics (IPK). The spatial distribution of the noise is determined using a 2D multi-group transport model in the time domain. Differently from the traditional point-kinetics approach, the angular flux is factorized into a shape $S(r, E, \Omega, t)$ and power $P(E, t)$ functions that preserve their energy dependence. More details on the IPK model formulation can be found in Brighenti et al. (2022).
- The diffusion-based solver CORE SIM+ (Mylonakis et al., 2021) and the transport-based solver NOISE-SN (Yi et al., 2021) developed by Chalmers University of Technology. The spatial distribution of the noise is determined via a solution of the two-energy group formulation in the frequency domain. The calculation of the spatial distribution of the neutron noise consists of two steps. In the first step, the fundamental eigenmode of the steady state problem is obtained. Then, in the second step, the neutron noise equations are solved in the frequency domain, using the static neutron flux and the multiplication factor previously evaluated and assuming no deviation of the perturbed system from criticality.

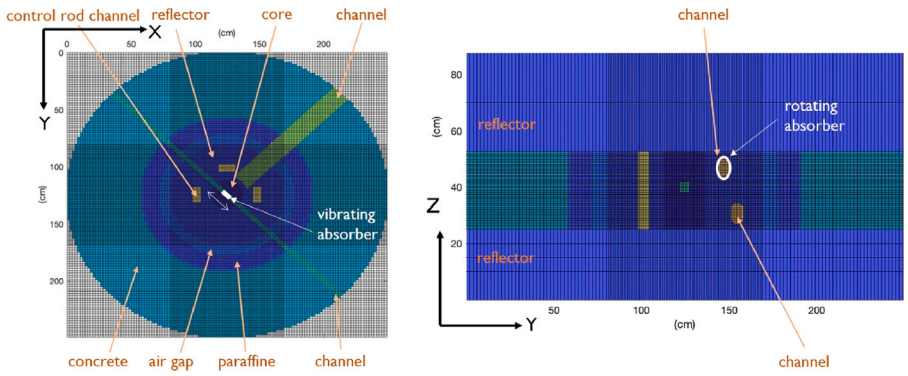

Fig. 7. CORE SIM+ model of the AKR-2 reactor.

Table 3
Summary of the noise models for the validation exercise.

Code	Models	Sol. to Bolz. Eq.	Sol. to Noise Eq.	Response	Detector model
TRIPOLI-4	CROCUS	Monte Carlo	Freq.	Reac. Rate	Yes
MCNP	AKR-2	Monte Carlo	Freq.	Reac. Rate	Yes
CORE SIM+	AKR-2, CROCUS	Diffusion	Freq.	Th. ϕ	No
APOLLO3	CROCUS	Det. Transport	Time Dep.	Reac. Rate	No
PARCS	CROCUS	Diffusion	Time Dep.	Th. ϕ	No
FEMFFUSION	CROCUS	Diffusion	Time Dep.	Th. ϕ	No
NOISE-SN	CROCUS	Det. Transport	Freq.	Th. ϕ	No

- The Monte Carlo solver developed by Kyoto University. The spatial distribution of the noise is determined based on a Monte Carlo solution of the continuous-energy transport equation in the frequency domain. The algorithm is similar to the one of TRIPOLI-4, but modifications are introduced to the particle flights instead of at collision events. Special functions for frequency domain calculation using complex-valued weights have been implemented into MCNP version 4 (Yamamoto, 2013, 2018).
- The diffusion-based solver FEMFFUSION (Vidal-Ferràndiz et al., 2020a) developed by Universitat Politècnica de València. The spatial distribution of the noise is determined based on a solution of the two-energy group diffusion equation in the time domain. This code also has implemented the SPN model. The noise sources (generic absorbers of variable strength and vibrating fuel assemblies) are modeled as time-dependent cross-sections.
- The diffusion-based code PARCS (Downar et al., 2002) was modified for noise analysis by Universitat Politècnica de València. The spatial distribution of the noise is determined based on a solution of the two-energy group diffusion model in the time domain. PARCS is a nuclear core simulator that solves the time-dependent two-group neutron diffusion equation in three-dimensional Cartesian geometry using nodal methods. For the modeling of vibrating fuel assemblies, an external module was developed to allow the use of customized time-dependent cross sections. The methodology used for these simulations is described in Vidal-Ferràndiz et al. (2020a).

A summary of the codes involved in the validation exercise for each reactor as well as the main features of the associated models is shown in Table 3. For each reactor, at least one deterministic and one Monte Carlo code are available. As a result, the effect on the bias of modeling the detector as well as the type of response considered can also be analyzed.

The computational uncertainty quantification is another key aspect of the validation exercise. For the needs of the CORTEX project, such analysis has been carried out only with CORE SIM+ for both AKR-2 and CROCUS. The computational uncertainties associated with the QoI are obtained using the GRS (Gesellschaft für Anlagen und Reaktorsicherheit) method (Kloos and Hofer, 1999). It consists in performing multiple calculations in which the code input and modeling parameters are varied according to their uncertainties. The number of calculations and thus the output sample size define the confidence level in the uncertainty estimates, as given by Wilks' formula (Wilks, 1991). In this work, the first and the fourth order Wilks' formulas for two-sided limits are selected, for the analysis of AKR-2 and CROCUS, respectively. These formulas require 93 and 260 samples of code runs each, to determine tolerance intervals with 95% confidence for the computational uncertainty due to the input parameters. The considered input parameters were nuclear data, technological parameters (fuel enrichment, pellet radius, etc.) as well as noise source parameters (amplitude, frequency, location). More details about the uncertainty and sensitivity analysis can be found in Yum et al. (2022).

4.1. Modeling the AKR-2 experiments

The three experimental campaigns at the AKR-2 reactors have been modeled with CORE SIM+ and MCNP. The respective reactor models are briefly described below.

4.1.1. CORE SIM+ model

The reactor is modeled as a collection of homogeneous regions, as illustrated in Fig. 7. The set of two-group homogenized nuclear constants for each region are generated with the Monte Carlo code Serpent (Leppänen et al., 2014).

Experiments involving both types of noise sources, namely the vibrating absorber and the rotating absorber, are modeled. The mesh is refined close to the location of the noise sources. No detectors are modeled in CORE SIM+, so the noise parameters are determined based on the thermal (up to 0.625 eV) neutron noise at the mesh location of the center of the active detector region.

Both noise sources are modeled exactly with a time-dependent expression of the thermal absorption macroscopic cross section fluctuations. The source description in the frequency domain is obtained by a Fourier transform of the time-dependent cross sections, keeping only the contribution of the excitation frequency ω_0 to define the source in the CORE SIM+ simulation. Due to the large size of the AKR-2 reactor compared to the size of the active core, numerical convergence is extremely challenging. The convergence properties of the model have been improved by using a multigrid preconditioner which is an extension of two-grid preconditioner described in Mylonakis et al. (2019).

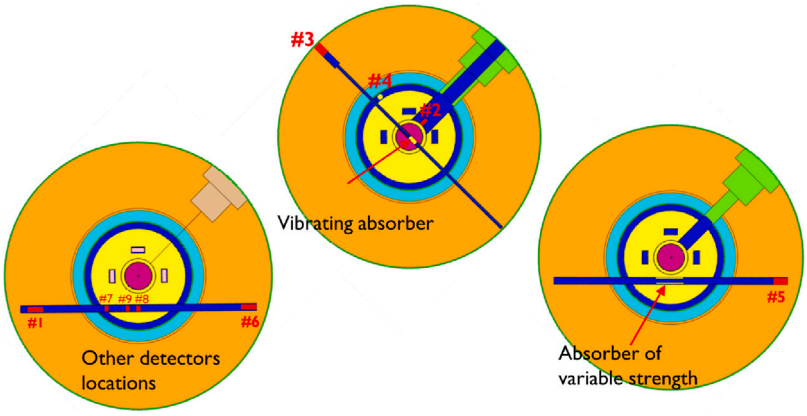

Fig. 8. MCNP model of the AKR-2 reactor.

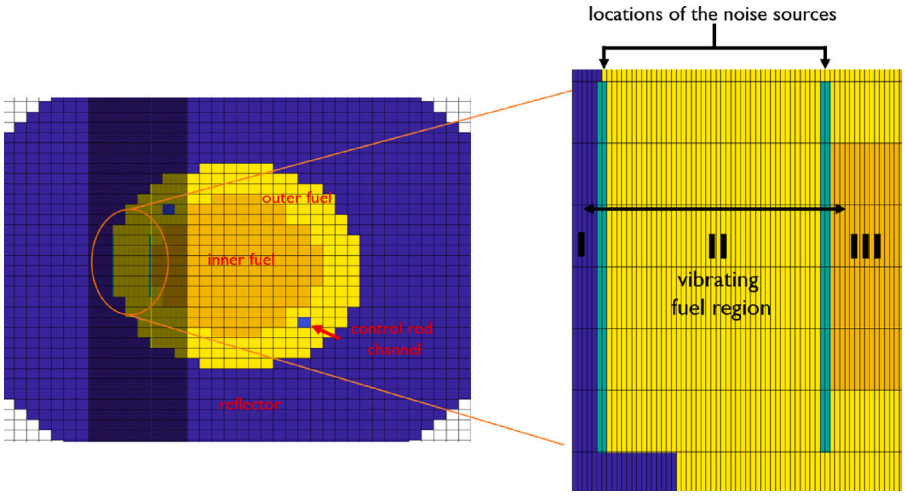

Fig. 9. CORE SIM+ model of the CROCUS reactor.

4.1.2. MCNP model

The MCNP models of the experiments at AKR-2 have been built specifically for the CORTEX project. An illustration of the MCNP models is shown in Fig. 8. The detectors are modeled explicitly, but their sizes and locations were adjusted (larger volume, position closer to the core) in order to improve the statistics of the noise particles during the Monte Carlo calculations and reduce the computing time. Typically, the number of histories (i.e., the number of complex-valued noise source particles) was 60,000,000 per experiment. Continuous-energy cross sections from the JENDL-4.0 nuclear data library were used.

The neutron noise source models used for MCNP are similar to the models developed for CORE SIM+, e.g. the total and scattering cross section fluctuations are represented in the time domain and transferred in the frequency domain through Fourier transform. Reaction rates of the complex-valued weights with the detector materials were calculated at each detector position.

4.2. Modeling the CROCUS experiments

The three experimental campaigns at the CROCUS reactor have been modeled with CORE SIM+, NOISE-SN, TRIPOLI-4, APOLLO3, FEMFFUSION and PARCS. The respective reactor models are briefly described below.

4.2.1. CORE SIM+ and NOISE-SN models

The CORE SIM+ 3D model of the CROCUS reactor core is illustrated in Fig. 9. It consists of three homogenized regions, i.e., the inner fuel region, the outer fuel region, and the water reflector. The two-group homogenized macroscopic neutron cross sections are generated using Serpent. This modeling approach was demonstrated to be faithful enough, at least for the calculation of the static neutron flux (Rais et al., 2017).

The modeling of the COLIBRI experiment is carried out using the ϵ/d method (Pázsit and Karlsson, 1997): the noise source is described by two Dirac-like perturbations localized at the boundaries of the region enclosing the moving fuel rods. The accuracy of the ϵ/d over the exact source model for each harmonic component has been described in Zoia et al. (2021). The differences between the macroscopic cross sections of the moving fuel regions and the neighboring regions dictate the amplitude of each perturbation. The mesh is refined around the moving fuel rods to accurately model the small fuel rods displacements.

No detectors are modeled in CORE SIM+, so the noise parameters are determined based on the thermal neutron noise at the mesh location of the center of the active detector region.

The NOISE-SN model is almost identical to the CORE SIM+ one, with minor differences in the mesh. An angular discretization corresponding to S_{16} is used, while the modeling of the noise source relies on the ϵ/d model.

4.2.2. FEMFFUSION and PARCS modeling

The FEMFFUSION and PARCS models of CROCUS are made of two-dimensional Cartesian grids. Each consists of a uniform mesh with square cells of 2.917 cm by 2.917 cm, i.e. the outer region pitch, which comprises COLIBRI. It is refined near the moving fuel region to allow

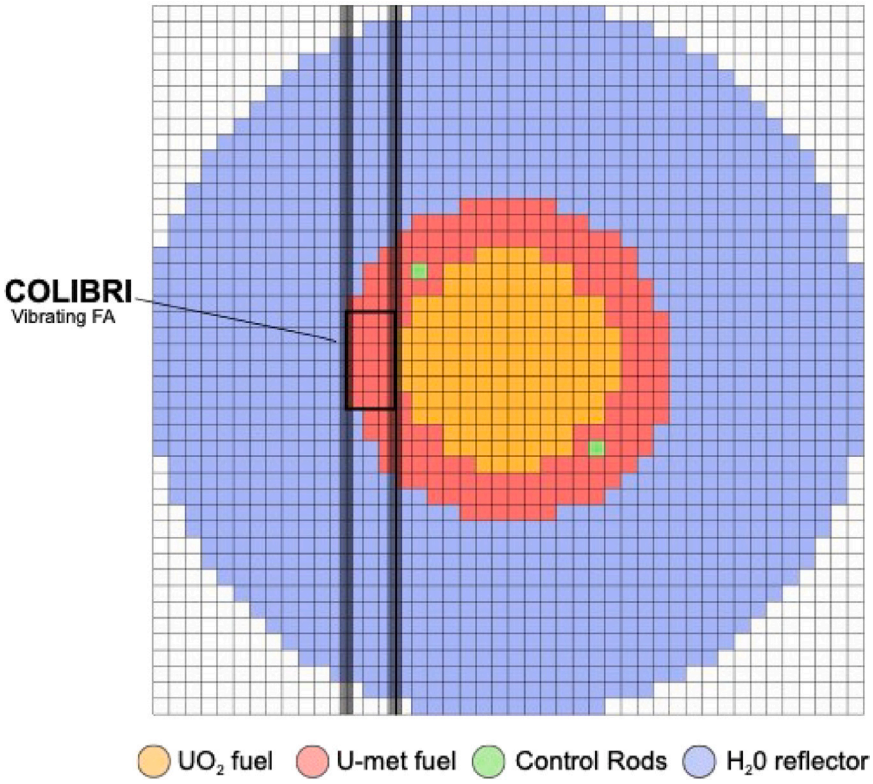

Fig. 10. PARCS/FEMFFUSION models of the COLIBRI experiment.

for an accurate modeling of the noise source. The mesh is illustrated in Fig. 10.

Similarly to the CORE SIM+ model, the homogenized cross sections and kinetic data were generated with Serpent using the approach described in Rais et al. (2017). The noise source modeling is described in details in Vidal-Ferràndiz et al. (2020b).

Three oscillations of each experiment were simulated in the time-domain using both diffusion and SP_3 solvers. The movement of the fuel rods was considered to be purely sinusoidal. As the differences between each time step are small, a fine spatial resolution and tight numerical convergence were required.

4.2.3. TRIPOLI-4 modeling

The TRIPOLI-4 noise calculations for the COLIBRI experiments have been documented in Vinai et al. (2021a). The main features of the CROCUS model are recalled here for completeness. A radial cut (mid-plane) of the CROCUS 3D model is shown in Fig. 11. The detectors are explicitly modeled. The 18 fuel pins of COLIBRI are modeled as 'square' cylinders to simplify the calculations of the noise source terms.

The TRIPOLI-4 calculations were performed using the JEFF3.1.1 nuclear data library. For the criticality calculations, 30'000 neutrons per batch are considered, and 100 batches were discarded. The noise calculations were carried out assuming 100'000 independent replicas. The noise source is modeled exactly through the Fourier transform of the fuel rods displacements (the ϵ/d approximation is not used). The COLIBRI movement is assumed to be purely monochromatic (the inertial effects in the COLIBRI vibrating mechanism are neglected). The noise parameters correspond to the detector reaction rate fluctuations and are determined in the active volumes of the detectors. For the Monte Carlo modeling of vibrating rods, the convergence of the solution for the noise amplitude at the frequency of interest is extremely slow. This issue stems from the fact that, because of the shape of the noise source for this class of noise problems, particle transport involves contributions with weights of opposite signs but nearly identical absolute value. Their sum, which yields the final noise tallies in the detectors, is then affected by a large variance.

4.2.4. APOLLO3 modeling

The APOLLO3 model for CROCUS and the COLIBRI experiments (Brighenti et al., 2022) is shown in Fig. 12. It is a 2D model where the axial neutron leakage is modeled through an axial buckling. The noise calculations are carried out in the time domain, and the detectors are explicitly represented. The noise parameters are based on the reaction rates computed in the active detector regions. A multi-group version of the JEFF-3.1.1 nuclear data library is used.

5. Validation exercise

In this section, the results of the validation exercises performed using the experimental data produced at AKR-2 and CROCUS are summarized.

In general, as reported in Yum et al. (2022), the computational uncertainties due to the input parameters of CORE SIM+, in both AKR-2 and CROCUS, are lower than the experimental uncertainties. For the AKR-2 experiments, they lie in the 0.1% range, the largest values being close to the noise source. For the CROCUS experiments, these values lie within the few % range for the detectors close to COLIBRI, and around 0.1–0.2% elsewhere. This phenomenon is due to the proximity of the noise source whose description is the leading source of computational uncertainty (Yum et al., 2022).

As a result, the computational uncertainties associated with the CORE SIM+ simulations will not be shown for the case studies at AKR-2 and CROCUS, even though they are available. The Monte Carlo statistical uncertainties are provided, however, as they are considerably larger and can sometimes attain the same magnitude as the experimental ones.

5.1. AKR-2 case study

The experimental parameters for the noise source associated with both measurements, as well as the specific measurement ID are listed in Table 1. The comparison of the QoI, simulated and measured, for the

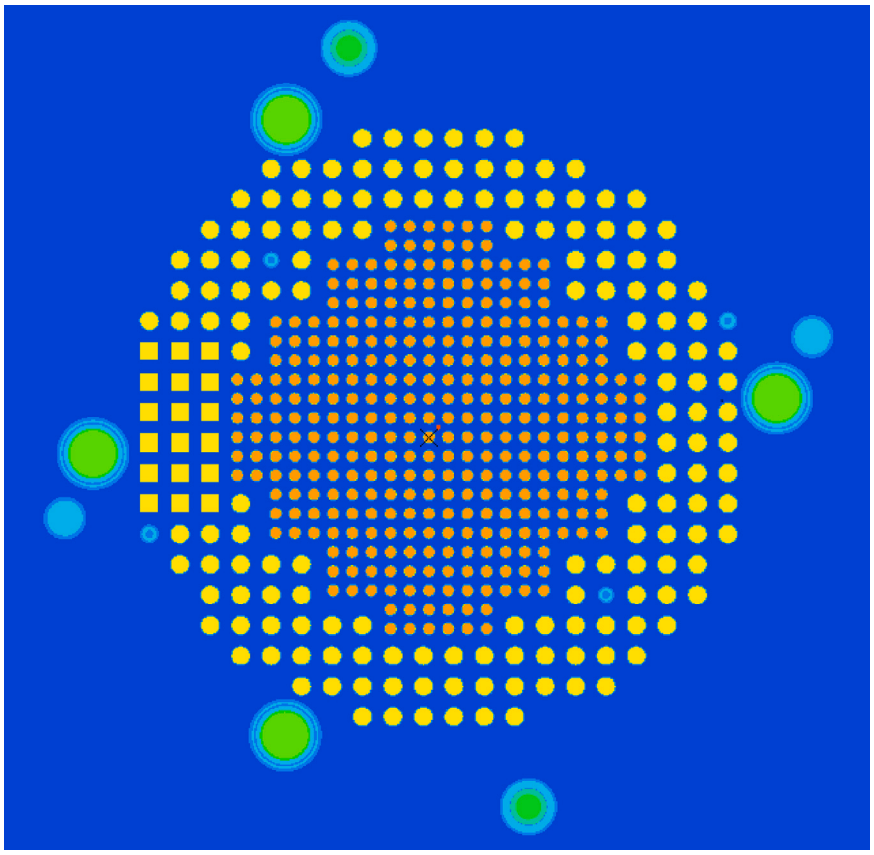

Fig. 11. Radial cut of the TRIPOLI-4 model of the CROCUS reactor.

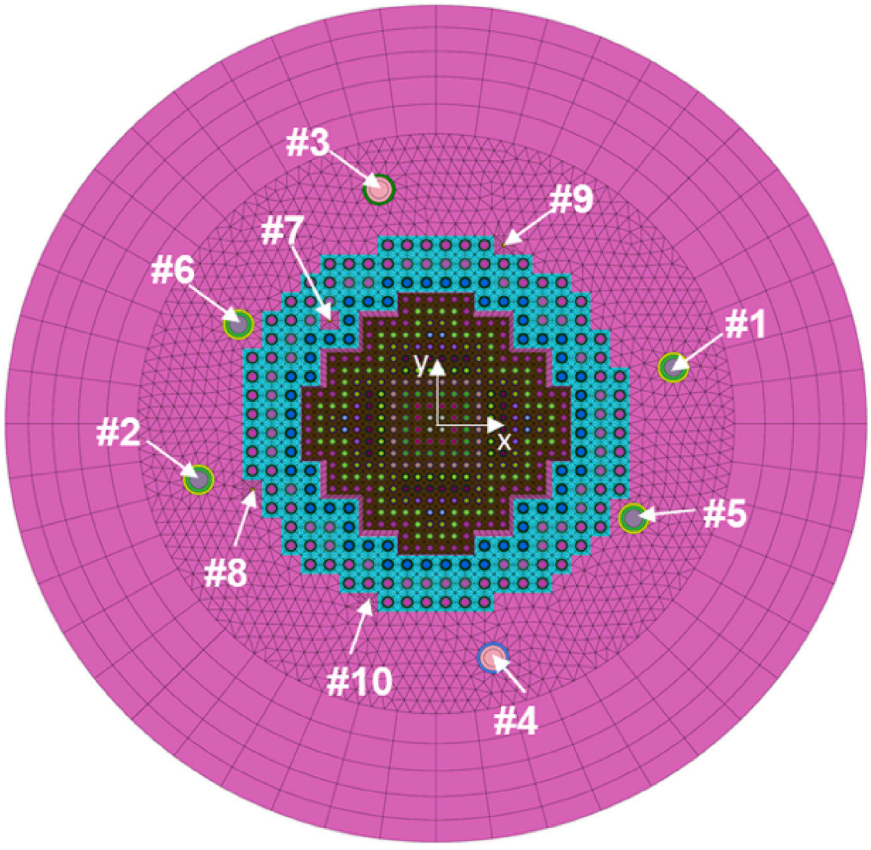

Fig. 12. APOLLO3 model of the CROCUS reactor.

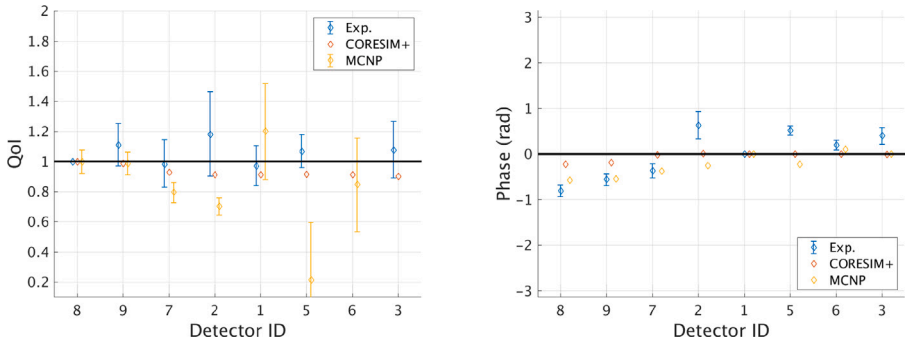

Fig. 13. Absorber of variable strength experiment at AKR-2; neutron noise amplitude (left) and phase (right). The computational uncertainties for the phase are negligible.

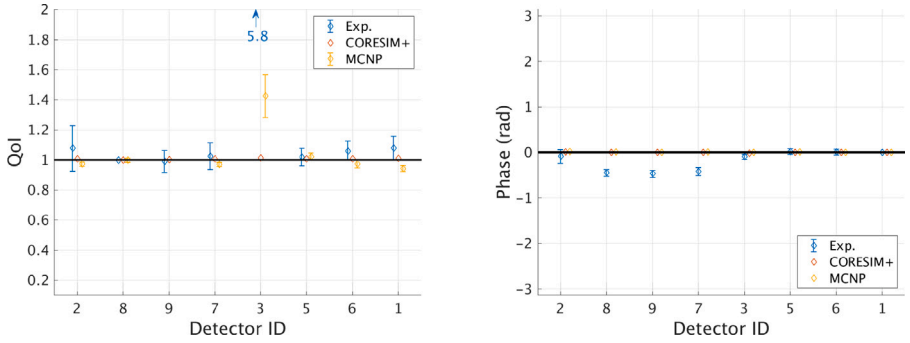

Fig. 14. Mechanical vibrations experiment at AKR-2; neutron noise amplitude (left) and phase (right).

two experiments considered at AKR-2 are shown in Fig. 13 for the AVS experiment and in Fig. 14 for the MV experiment. The experimental data shown is one occurrence of a measurement repeated a number of times (see 1). As the spread of the experimental results through their repetition fits within the experimental uncertainties, this choice is arbitrary and does not impact the conclusion of the case study.

Due to convergence issues with the Monte Carlo solution, the detector #8 is chosen as reference for the AVS experiment as it is closer to the core. As a result, the QoI will be lower than one for detectors further away from the noise source. However, this does not change the implications of a deviation of the QoI from 1.0: it is still a sign of a non-zero spatial component of the relative noise. With respect to the representation of the results in Figs. 13 and 14, the noise parameters (QoI and phase) for the various models and the associated measurements are shown on the y-axis at each considered detector location. On the x-axis, the detectors are sorted out by their distance to the noise source, e.g. in Fig. 13, the detector #8 is closer to the noise source than detector #9. Even though the detector location does not change during a given experimental campaign, their order might differ depending on the type of noise source considered, since the AVS and MV have different locations as described in Section 3. The location of each detector (and their corresponding ID) is shown in Fig. 4.

When considering the AVS experiment, the QoI calculated with MCNP and CORE SIM+ are consistent with the experimental results in the limit of the large uncertainties involved. The CORE SIM+ results suggest that the spatial component of the relative noise exists with deviations from 1.0 of the QoI in the 10%–15% range. Close to the core, the trends of CORE SIM+ are confirmed by MCNP. However, due to difficulties in converging the Monte Carlo solution, the Monte Carlo uncertainties are large for the detectors further away, e.g. #5, #6 and #3. The experimental uncertainties were reduced during the third experimental campaign at AKR-2, as illustrated in Fig. 5, but not to a level where the deviations from one observed with the simulations could be confirmed by measurements.

Unexpected phase differences in the radian range are observed in the experimental data for certain detectors. These deviations are due to synchronization issues reported during the second campaign at AKR-2 (see Section 3) and are not meaningful.

With respect to the MV experiment, the QoI calculated with MCNP and CORE SIM+ is close to unity for most of the detectors and agrees well with the experimental results. The spatial component of the relative noise appears to be too small to be resolved. The deviations from 1.0 of the QoI are <1% when considering the CORE SIM+ results.

For the detector #3, which is located far from the core, in the same reactor channel as the noise source, the experimental value for the QoI is equal to 5.8[1]; the MCNP calculation appears to partially capture the QoI increase, while the CORE SIM+ model does not. This is a clear indication that the spatial component of the relative noise is visible for this detector. It is to be noted that, although far from the active core, detector #3 is located in the channel crossing the core, where the MV is set as well.

Similarly to the AVS experiment, unexpected phase differences in the radian range are observed in the experimental data for certain detectors. These deviations are due to synchronization issues reported during the second campaign at AKR-2 (see Section 3) and are again not meaningful.

In summary, the codes managed to capture the noise behavior in AKR-2. Due to the detector positions being far from the active core, the uncertainties could not be reduced enough, especially in the AVS case, to capture experimentally the spatial component of the relative noise, except in the specific case of detector #3 in the MV experiment.

5.2. CROCUS case study

The experimental parameters for the noise source associated with the three measurements, as well as the specific measurement ID, are

[1] This is not an outlier, as the magnitude of the QoI is confirmed by repetitions of the measurement during two campaigns.

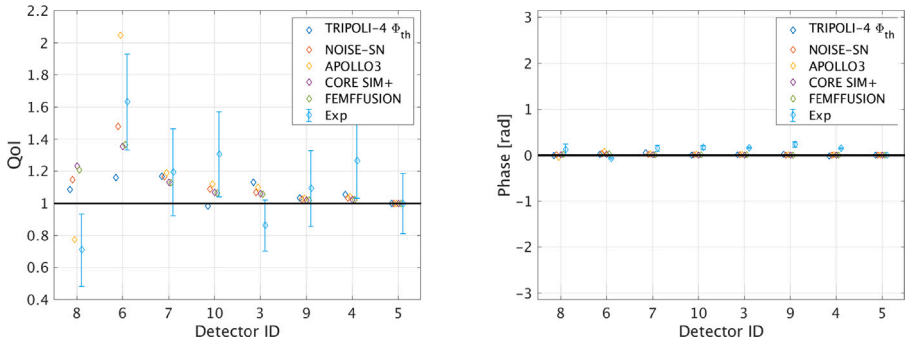

Fig. 15. Experiment 13 during the first experimental campaign at CROCUS; QoI (left) and phase (right). The detector #5 is used as reference.

listed in Table 2. Similarly as for the AKR-2 case study, the experimental data selected for representation is a specific repetition of the measurement.

The first experiment considered here took place during the first campaign at CROCUS. The QoI and phase are shown in Fig. 15. The results calculated with diffusion-based solvers such as CORE SIM+, FEMFFUSION and PARCS are similar and agree with NOISE-SN (based on a discrete ordinates method) and with FEMFFUSION-SP3. This is expected, as these simulations make use of very similar reactor models. For the sake of readability, the SP3 solutions of PARCS and FEMFFUSION as well as the diffusion solution of PARCS are not shown in Fig. 15.

The solvers predict a similar behavior for the neutron noise, i.e., an increase of the QoI close to the oscillating fuel rods (from detector #8 to detector #6) and a decrease in other locations that are further from the perturbation (from detector #6 to detector #5). Due to the large experimental uncertainties, no significant bias between the models and the measurement can be observed. Aside from detector #6 (having more than 60% deviation), a possible spatial component of the relative noise is hidden in the experimental uncertainties, even though the simulations suggest that deviations in the 10%–20% range should be observed for detectors #7, #10 and #3. The phase difference with respect to the reference detector #5 is approximately zero at any of the available detector locations; both simulations and measurements provide consistent results.

A few additional points can be made based on the code-to-code comparison. First, while the models are fairly consistent far from the noise source, larger discrepancies are found for detectors #8 and #6. They are possibly due to neutron transport and spectral effects, which may be challenging to be properly taken into account in the region close to the perturbation.

The APOLLO3 model allows for an accurate modeling of the real COLIBRI oscillations (see Brighenti et al., 2022 for details); this leads to significant differences close to the perturbation (detectors #8 and #6) with respect to the other solvers.

The second and third experiments considered in this case study took place during the second campaign at CROCUS. The QoI and phase are shown in Figs. 16 and 17 for 0.1 Hz and 1 Hz oscillations, respectively.

For both experiments, the simulations and the measurements yield a similar behavior for the neutron noise, although discrepancies are again found near the noise source.

For the detector #2, which is located close to the source, the experimental value for the QoI is equal to 3.4 for the low and high frequency measurements. It is not included in the plot.

Statistically significant deviations from one for the QoI are observed in the experimental results and confirmed by the models. The deviations are in the 10 to 15% range far from the source (detector #5 and further). A non-zero spatial component of the relative noise is visible in CROCUS even relatively far from the noise source. The numerical simulations appear to capture it well.

The phase is negligible away from the noise source. Both measurements and simulations are consistent in this respect. In the experimental results, a statistically significant deviation from zero is observed at 1 Hz (it is less clear at 0.1 Hz, due to the larger experimental uncertainty) for the detector located behind the COLIBRI device with respect to the core (detector #14).

With respect to the comparison of the simulation results, TRIPOLI-4 predicts a decrease of neutron noise amplitude from detector #8 to detector #14, an increase from detector #14 to detector #2, and a monotonic decrease when the distance to the noise source increases. The diffusion-based solvers CORE SIM+ and FEMFFUSION yield a maximum of the QoI at the location of detector #2, followed by a monotonic decrease when moving further away from the noise source. Possible discrepancies close to the noise source (e.g., at the locations of detectors #8 and #14) may be due to well-known limitations of diffusion theory close to sources.

The results obtained with TRIPOLI-4, considering QoI based on either the reaction rates or the thermal flux, are almost identical but differ at the position of detectors #8 and #14, which are closest to the noise source and as such are probably sensitive to spectral effects.

6. Conclusions

In this paper we have illustrated the validation activities carried out within the CORTEX project, targeting the neutron noise solvers used or developed within the project. Models of the research reactors AKR-2 and CROCUS for the various solvers have been produced to simulate the neutron noise experiments carried out at both facilities. After the description of meaningful and convenient quantities of interest for the purpose of CORTEX, an in-depth comparison of the models and measurements has been reported.

At AKR-2, measurements were carried out with two types of noise sources and modeled with diffusion-based and transport-based solvers in the frequency domain. The reactor is extremely challenging to model from a deterministic point of view because of the location of the detectors with respect to the core; and to the presence of experimental channels. Converging the Monte Carlo solution was also difficult, especially for the AVS experiments. Overall, the codes managed to capture the main features of the noise behavior in AKR-2. Due to the detector positions being far from the core, the experimental uncertainties could not be reduced, especially in the AVS case, to a level allowing having experimental evidences that the spatial component of the relative noise was non-zero. However, local effects were observed in some specific conditions, e.g. for detectors facing the noise source. It was found that diffusion-based solvers are not adequate for the modeling of such features.

Next, a selection of COLIBRI experiments at CROCUS were modeled using a variety of codes both in the frequency and time domain, using the transport and diffusion theory. In terms of spatial effects, statistically significant deviations from one for the QoI were observed experimentally, even relatively far from the noise source. This was achieved through long irradiation periods and the possibility to install detectors in the near vicinity or inside the CROCUS core. A significant

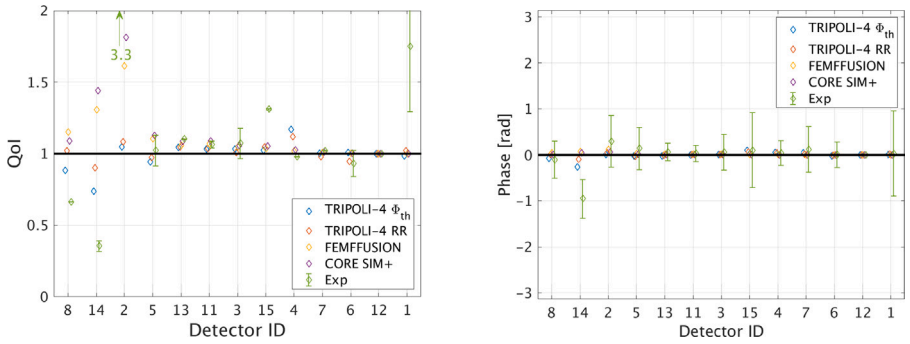

Fig. 16. Experiment 7 during the second experimental campaign at CROCUS; QoI (left) and phase (right). The detector #12 is used as reference.

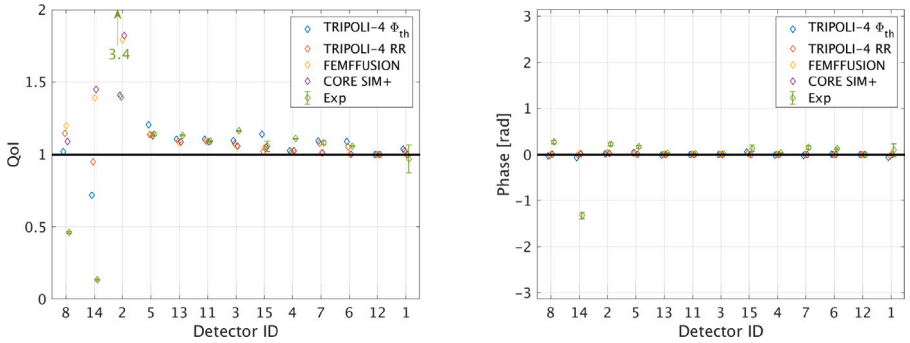

Fig. 17. Experiment 8 during the second experimental campaign at CROCUS; QoI (left) and phase (right). The detector #12 is used as reference.

phase difference between detectors could be recorded when placing the detectors close enough to either sides of the COLIBRI vibrating fuel rods. Both points suggest that the spatial component of the relative noise is visible in the CROCUS reactor, despite its compact size. The solvers managed to capture the noise behavior in CROCUS, except close to the noise source.

Modeling the detector and considering the reaction rates instead of the thermal flux QoI does not appear to lead to large differences, as long as the detector is located sufficiently far from the noise source. The use of diffusion instead of transport theory does not result in a large accuracy loss far from the source; however, clear differences are observed close to the noise source. The conclusions are similar when considering time or frequency domain calculations. The use of a time domain approach allows for a more accurate description of the noise source, for example the non-sinusoidal movement of COLIBRI.

In CORTEX, the experimental data for code validation has produced using zero-power research reactors. This allowed the production of earmarked data which could be used to test the performance of the machine-learning algorithms. Admittedly, due to their size, to the lack of thermal-hydraulic feedback and to the use of fresh fuel, zero-power research reactors are not representative of power reactors. The noise sources also differ: neutron population fluctuations are artificially produced through the introduction of a mechanical vibration or an absorber of variable strength. This clearly limits the representativeness of the measurements in terms of direct applicability to noise problems in power reactors, for which further investigations will be required.

However, with respect to the objectives of this paper, i.e. demonstrating that the noise simulators produce a reliable description of the noise field in a reactor, the limitations reported for the considered models of CROCUS and AKR-2 may not be an issue for the analysis of large power reactors. Indeed, most of the issues with the models are found close to the source. In power reactor analysis, the noise sources will be further away from the detectors, and the magnitude of the spatial component should be much larger. In a sense, modeling the spatial variations of the relative neutron noise behavior in zero-power research reactors is an extremely challenging problem because of the small magnitude of the spatial component; and because it is most visible in small reactors through distinct features of the core which are hard to model, e.g. within the experimental channels.

CRediT authorship contribution statement

M. Hursin: Conceptualization, Writing. **A. Zoia:** Methodology, Writing. **A. Rouchon:** Investigation. **A. Brighenti:** Investigation. **I. Zmijarevic:** Supervision. **S. Santandrea:** Supervision. **P. Vinai:** Methodology, Writing. **A. Mylonakis:** Investigation. **H. Yi:** Investigation. **C. Demazière:** Methodology, Writing, Funding acquisition. **V. Lamirand:** Investigation. **K. Ambrozic:** Investigation, Writing. **T. Yamamoto:** Investigation. **S. Hübner:** Investigation. **A. Knospe:** Investigation, Writing. **C. Lange:** Supervision. **S. Yum:** Investigation. **R. Macian:** Supervision. **A. Vidal:** Investigation, Writing. **D. Ginestar:** Supervision, Writing. **G. Verdú:** Supervision.

Declaration of competing interest

The authors declare that they have no known competing financial interests or personal relationships that could have appeared to influence the work reported in this paper.

Data availability

Data will be made available on request

Acknowledgments

The CORTEX research project has received funding from the Euratom research and training program 2014–2018 under grant agreement No 754316.

References

Adorjan, F., Czibok, T., Kiss, S., Krinizs, K., Vegh, J., 2000. Core asymmetry evaluation using static measurements and neutron noise analysis. Ann. Nucl. Energy 27, 649–658.

Alexandridis, G., 2020. Results of the application and demonstration calculations. CORTEX Deliv. D4.4, 72, URL https://cortex-h2020.eu/wp-content/uploads/2020/08/CORTEX-D4.4-Results-of-the-application-and-demonstration-calculations.pdf.

Ambrozic, K., 2021. Characterization of high harmonic frequencies in reactor noise experimentswithin the CORTEX project. In: ANIMMA.

Ambrožič, K., Lamirand, V., Knospe, A., Vitullo, F., Hübner, S., Pakari, O., Hursin, M., Rais, A., Lange, C., Laureau, A., Frajtag, P., Fiorina, C., Pautz, A., 2023. Postprocessing of experimental time series to determine reliable mean and uncertainties. ANE http://dx.doi.org/10.1016/s1537-1891(09)00089-5, under review.

Brighenti, A., Santandrea, S., Zmijarevic, I., Stankovski, Z., 2022. Development and validation of a time-dependent deterministic model for neutron noise on CROCUS experimental measurements. Ann. Nucl. Energy 165, 108753. http://dx.doi.org/10.1016/j.anucene.2021.108753.

Demazière, C., Vinai, P., Hursin, M., Kollias, S., Herb, J., 2018. Overview of the cortex project. In: PHYSOR 2018: Reactor Physics Paving the Way Towards more Efficient Systems. Cancun, Mexico.

Downar, T.J., Barber, D.A., Matthew Miller, R., Lee, C.-H., Kozlowski, T., Lee, D., Xu, Y., Gan, J., Joo, H.G., Cho, J.Y., Lee, K., Ulses, A.P., 2002. PARCS: Purdue advanced reactor core simulator. In: Proceedings of the PHYSOR 2002 - International Conference on the New Frontiers of Nuclear Technology : Reactor Physics, Safety and High-Performance Computing - the ANS 2002 RPD Topical Meeting. URL https://www.scopus.com/inward/record.uri?eid=2-s2.0-85093912932{&}partnerID=40{&}md5=a7f07c4e27ad8f103a01f47453c8d5ad.

Heideman, M., Johnson, D., Burrus, C.S., 1984. Gauss and the history of the fast fourrier transform. IEEE Signal Process. Mag. 1 (3), 14–21.

Hübner, S., 2018. Neuauslegung, Inbetriebnahme und Test eines hochpräzisen Pile-Oszillators für den AKR-2 (Ph.D. thesis). Technische Universitaet Dresden.

Hübner, S., Knospe, A., Viebach, M., Lange, C., Hurtado, A., 2020. Experimental determination of the zero power transfer function of the AKR-2. In: International Conference on Physics of Reactors: Transition to a Scalable Nuclear Future, PHYSOR 2020, Vol. 2020-March. pp. 2955–2962. http://dx.doi.org/10.1051/epjconf/202124721009.

Kloos, M., Hofer, E., 1999. SUSA - PC, a personal computer version of the program system for uncertainty and sensitivity analysis of results from computer models, version 3.2.

Lamirand, V.P., Ambrožič, K., Knospe, A., Hübner, S., 2023a. Experimental campaigns at AKR-2 and CROCUS. Ann. Nucl. Energy submitted for publication.

Lamirand, V.P., Ambrožič, K., Pakari, O.V., Vitullo, F., Rais, A., Laureau, A., Hursin, M., Fiorina, C., Frajtag, P., Pautz, A., 2023b. Results of the noise experimental campaigns in CROCUS for the European project CORTEX. Ann. Nucl. Energy submitted for publication.

Lamirand, V., Frajtag, P., Godat, D., Pakari, O., Laureau, A., Rais, A., Hursin, M., Perret, G., Fiorina, C., Pautz, A., 2020a. The COLIBRI experimental program in the CROCUS reactor: characterization of the fuel rods oscillator. EPJ Web Conf. 225, 04020. http://dx.doi.org/10.1051/epjconf/202022504020.

Lamirand, V., Hübner, S., Pakari, O., Vitullo, F., Ambrožič, K., Knospe, A., Rais, A., 2020b. Experimental report of the 2nd campaign at AKR-2 and CROCUS. CORTEX Deliv. D2.2, 32, URL https://cortex-h2020.eu/wp-content/uploads/2021/03/CORTEX-D2.2-experimental-report-of-the-2nd-campaign-at-AKR-2-and-CROCUS-V2.pdf.

Lamirand, V., Hursin, M., Rais, A., Hübner, S., Lange, C., Laureau, A., Pohlus, J., Paquee, U., Pohl, C., Pakari, O., 2018. Experimental report of the 1st campaign at AKR-2 and CROCUS. CORTEX Deliv. D2.1, 32, URL https://cortex-h2020.eu/wp-content/uploads/2019/07/CORTEX_D2_1_Experimental_Report_of_the_1st_Campaign_at_AKR2_and_CROCUS_V1.pdf.

Lamirand, V., Knospe, A., Ambrožič, K., Vitullo, F., Lange, C., 2021. Experimental report of the 3rd campaign at AKR-2 and CROCUS. CORTEX Deliv. (D2.4), 32, URL https://cortex-h2020.eu/wp-content/uploads/2021/09/CORTEX_D2_4_Experimental_report_of_the_3rd_campaign_at_AKR_2_and_CROCUS_V1.pdf.

Lamirand, V., Rais, A., Hübner, S., Lange, C., Pohlus, J., Paquee, U., Pohl, C., Pakari, O., Frajtag, P., Godat, D., Hursin, M., Laureau, A., Perret, G., Fiorina, C., Pautz, A., 2020c. Neutron noise experiments in the AKR-2 and CROCUS reactors for the European project CORTEX. EPJ Web Conf. 225, 04023. http://dx.doi.org/10.1051/epjconf/202022504023.

Leppänen, J., Pusa, M., Viitanen, T., Valtavirta, V., Kaltiaisenaho, T., 2014. The serpent Monte Carlo code: status, development and applications in 2013. In: SNA + MC 2013 - Joint International Conference on Supercomputing in Nuclear Applications + Monte Carlo. EDP Sciences, p. 6021. http://dx.doi.org/10.1051/snamc/201406021, URL https://sna-and-mc-2013-proceedings.edpsciences.org/articles/snamc/abs/2014/01/snamc2013{_}06021/snamc2013{_}06021.html.

Mylonakis, A., Vinai, P., Demazière, C., 2019. Two-level multigrid preconditioning of a neutron noise diffusion solver. In: International Conference on Mathematics and Computational Methods Applied to Nuclear Science and Engineering, M&C 2019. pp. 1208–1217.

Mylonakis, A., Vinai, P., Demazière, C., 2021. CORE SIM+: A flexible diffusion-based solver for neutron noise simulations. Ann. Nucl. Energy 155, 108149. http://dx.doi.org/10.1016/j.anucene.2021.108149.

Pázsit, I., 1977. Investigation of the space-dependent noise induced by a vibrating absorber. Atomkernenergie (ATKE) 30.

Pázsit, I., Demazière, C., 2010. CRC- chapter 14 noise techniques in nuclear systems. In: Handbook of Nuclear Engineering. Springer, Boston, MA.

Pázsit, I., Karlsson, J., 1997. On the perturbative calculation of the vibration noise by strong absorbers. Ann. Nucl. Energy 24 (6), 449–466. http://dx.doi.org/10.1016/S0306-4549(96)00081-3.

Rais, A., Lamirand, V., Pakari, O., Laureau, A., Pohlus, J., Pohl, C., Hübner, S., Hursin, M., Demazière, C., Pautz, A., 2019. Towards the validation of neutron noise simulators: qualification of data acquisition systems. In: International Conference on Mathematics and Computational Methods Applied to Nuclear Science and Engineering.

Rais, A., Siefman, D.J., Hursin, M., Ward, A., Pautz, A., 2017. Neutronics modeling of the crocus reactor with serpent and parcs codes. In: International Conference on Mathematics and Computational Methods Applied To Nuclear Science and Engineering.

Rouchon, A., Jarrah, W., Zoia, A., 2019. The new neutron noise solver of the Monte Carlo code tripoli-4®R. In: International Conference on Mathematics and Computational Methods Applied to Nuclear Science and Engineering, M and C 2019. pp. 332–341.

Rouchon, A., Zoia, A., Sanchez, R., 2017. A new Monte Carlo method for neutron noise calculations in the frequency domain. Ann. Nucl. Energy 102, 465–475. http://dx.doi.org/10.1016/j.anucene.2016.11.035.

Stefanos, K., Stafylopatis, A., Leontidis, G., Alexandridis, G., Tabouratzis, T., Durrant, A., 2020. Development of machine learning techniques and evaluation of analysis results. CORTEX Deliv. D3.4, URL https://cortex-h2020.eu/wp-content/uploads/2020/04/CORTEX_D3_4_Development_of_machine_learning_techniques_and_evaluation_of_analysis_results_V1.pdf.

Stulík, P., Torres, L.A., Montalvo, C., Garcia-Berrocal, A., Salazar, C., Alexandridis, G., Tabouratzis, T., Machek, J., Pantera, L., Bem, M., 2019. Development of advanced signal processing techniques and evaluation results. CORTEX Deliv. D3.3, 108, URL https://cortex-h2020.eu/wp-content/uploads/2020/04/CORTEX_D3_3_Development_of_advanced_signal_processing_techniques_and_evaluations_V1.pdf.

Vidal-Ferràndiz, A., Carreño, A., Ginestar, D., Demazière, C., Verdú, G., 2020a. A time and frequency domain analysis of the effect of vibrating fuel assemblies on the neutron noise. Ann. Nucl. Energy 137, http://dx.doi.org/10.1016/j.anucene.2019.107076.

Vidal-Ferràndiz, A., Demazière, C., Dokhane, A., Ginestar, D., Knospe, A., Kuentzel, M., Mylonakis, A., Perin, Y., Lange, C., Verdu, G., Verma, V., Vinai, P., 2020b. Modelling of the neutron flux response to vibrating fuel assemblies. CORTEX Deliv. D1.3, URL https://cortex-h2020.eu/wp-content/uploads/2021/03/CORTEX_D1_3_Modelling_of_the_neutron_flux_response_to_vibrating_fuel_assemblies_V1.pdf.

Vidal-Ferràndiz, A., Ginestar, D., Carreño, A., Verdú, G., Dokhane, A., Verma, V., Perin, Y., Herb, J., Mylonakis, A., Demazière, C., Vinai, P., 2022. Modelling and simulations of reactor neutron noise induced by mechanical vibrations. Ann. Nucl. Energy 177, http://dx.doi.org/10.1016/j.anucene.2022.109300.

Vinai, P., Brighenti, A., Demazière, C., Gasse, B., Ginestar, D., Mylonakis, A.G., Rouchon, A., Santandrea, S., Tatidis, A., Vidal-Ferràndiz, A., Verdu, G., Yamamoto, T., Yi, H., Zmijarevic, I., Zoia, A., 2021a. Development and comparison of highorder solvers for reactor noise analysis. CORTEX Deliv. D1.4, URL https://cortex-h2020.eu/wp-content/uploads/2021/09/CORTEX_D1_4_Development_and_comparison_of_highorder_solvers_for_reactor_noise_analysis_V1.pdf.

Vinai, P., Yi, H., Demazière, C., Rouchon, A., Zoia, A., Vidal-Ferràndiz, A., Carreño, A., Ginestar, D., Verdú, G., 2023. On the simulation of neutron noise induced by vibrations of fuel pins in a fuel assembly. Ann. Nucl. Energy 181 (September 2022), http://dx.doi.org/10.1016/j.anucene.2022.109521.

Vinai, P., Yi, H., Mylonakis, A., Demazière, C., Gasse, B., Rouchon, A., Zoia, A., Ferràndiz, A., Ginestar, D., Verdú, G., Yamamoto, T., 2021b. Comparison of neutron noise solvers based on numerical benchmarks in a 2-D simplified UOX assembly. In: International Conference on Mathematics and Computational Methods Applied to Nuclear Science and Engineering (M&C 2021). pp. 2016–2025.

Vincent, L., Vitullo, F., Klemen Ambrozic, Pakari, O.V., Braun, L., Godat, D., 2021. Report on the development of fibre-based scintillator. CORTEX Deliv. D2.3, URL https://cortex-h2020.eu/wp-content/uploads/2021/03/CORTEX-D2{_}3{_}report{_}on{_}the{_}development{_}of{_}fibre{_}based{_}scintillator.pdf.

Vitullo, F., Lamirand, V., Mosset, J.-b., Frajtag, P., Pakari, O., Perret, G., Pautz, A., 2020. A mm3 fiber-coupled scintillator for in-core thermal neutron detection in CROCUS. IEEE Trans. Nucl. Sci..

Wilks, S.S., 1991. Determination of sample sizes for setting tolerance limits. Ann. Math. Stat..

Yamamoto, T., 2013. Monte Carlo method with complex-valued weights for frequency domain analyses of neutron noise. Ann. Nucl. Energy 58, 72–79. http://dx.doi.org/10.1016/j.anucene.2013.03.002, URL http://www.sciencedirect.com/science/article/pii/S0306454913001229.

Yamamoto, T., 2018. Implementation of a frequency-domain neutron noise analysis method in a production-level continuous energy Monte Carlo code: Verification and application in a BWR. Ann. Nucl. Energy 115, 494–501. http://dx.doi.org/10.1016/j.anucene.2018.02.008.

Yi, H., Vinai, P., Demazière, C., 2021. On the simulation of neutron noise using a discrete ordinates method. Ann. Nucl. Energy 164, 108570. http://dx.doi.org/10.1016/j.anucene.2021.108570.

Yum, S., Hursin, M., Vasiliev, A., Vinai, P., Mylonakis, A.G., Demazière, C., Macián-juan, R., 2022. Uncertainty analyses of neutron noise simulations in a zero-power reactor. Ann. Nucl. Energy 174, 109157. http://dx.doi.org/10.1016/j.anucene.2022.109157.

Zoia, A., Rouchon, A., Gasse, B., Demazière, C., Vinai, P., 2021. Analysis of the neutron noise induced by fuel assembly vibrations. Ann. Nucl. Energy 154, 108061. http://dx.doi.org/10.1016/j.anucene.2020.108061.